ELSEVIER

Journal of Nuclear Materials 249 (1997) 175–189

journal of nuclear materials

Measurement of kinetic rate law parameters on a Na–Ca–Al borosilicate glass for low-activity waste

B.P. McGrail [a,*], W.L. Ebert [b], A.J. Bakel [b], D.K. Peeler [c]

[a] *Applied Geology and Geochemistry Department, Pacific Northwest National Laboratory, Richland, WA 99352, USA*
[b] *Chemical Technology Department, Argonne National Laboratory, Argonne, IL 60439, USA*
[c] *Westinghouse Savannah River Company, Aiken, SC 29808 USA*

Received 28 October 1996; accepted 9 June 1997

Abstract

The dissolution kinetics of a Na–Ca–Al borosilicate glass, being studied for immobilization of low-activity waste, were measured between 20 and 90°C and solution pH between 6 and 12 using the single-pass flow-through method. Dissolution kinetics measurements are needed to parameterize a mechanistic model that is being used to compute the corrosion rate of the glass waste form as a function of temperature, pH, and the concentrations of the other glass components in water percolating through a proposed shallow-land disposal facility. The key factors that were found to influence the test results include test duration and background subtraction of the raw data. Background subtraction is shown to be important to prevent a non-physical increase in the computed rate with increasing flow rate, particularly in tests run at higher flow rates. Experimental factors that were found to have no detectable influence on the test results included the glass particle size and buffer type. We also illustrate how flow rate variations can be used to obtain information about the reaction order and equilibrium constant parameters in a conventional transition-state theory rate law. © 1997 Elsevier Science B.V.

1. Introduction

Retrieval and treatment of highly radioactive wastes stored in underground tanks at Hanford in the state of Washington are planned that will generate both a high-level and a low-activity waste stream. The low-activity fraction will be vitrified and disposed in a shallow-land burial facility on the Hanford site that will contain as much as 550 000 metric tons of glass. Before the disposal action can proceed, quantitative radionuclide release calculations must be performed to provide assurance that the facility design will protect groundwater resources and public health and safety over very long time periods. These calculations will be done with the aid of computer codes. The Analyzer of Radionuclide Source-Term with Chemical Transport (AREST-CT) code, developed at Pacific Northwest National Laboratory (PNNL) for the US Department of Energy for evaluation of arid land disposal sites, was selected in 1995 as the computer code that will be used to perform quantitative radionuclide release estimates from the LAW disposal facility [1]. The AREST-CT code [2] is one of a new generation of so-called reactive chemical transport codes that allow the simultaneous simulation of solute transport modified by both equilibrium and kinetically-constrained chemical reactions. In this paper, we present results from a set of experimental studies on a Na–Ca–Al borosilicate glass designed to parameterize a kinetic rate law that has been implemented in the AREST-CT code to describe the corrosion rate of glass waste forms in a disposal system.

* Corresponding author. Tel.: +1-509 376 9193; fax: +1-509 376 2210; e-mail: pete.mcgrail@pnl.gov.

PII S0022-3115(97)00213-4

2. Background

The corrosion of silicate glasses in water can be represented as a special type of irreversible dissolution reaction. A conventional transition state kinetic rate equation [3] can be used to compute the flux of any element i released from the glass into the aqueous phase and is given by

$$J_i^a = \upsilon_i \vec{k} e^{-\frac{E_a}{RT}} \left[1 - \left(\frac{Q}{K}\right)^{\sigma}\right] \prod_j a_j^{-\eta_j}, \quad i = 1, 2, \ldots, N, \tag{1}$$

where a_j is the activity of jth aqueous species, $\vec{k}$ is the intrinsic rate constant (g/m^2 s), E_a is activation energy (J/mol), J_i^a is the flux of element i (g/m^2 s), K is the equilibrium constant of rate controlling phase, N is the number of elements, Q is the ion-activity product of rate controlling phase, R is the gas constant (J/mol/K), T is temperature (K), υ_i is the stoichiometric coefficient of element i in the glass, σ is the net reaction order, and η_j is thestoichiometric coefficient for the jth reactant species.

Eq. (1) is a constitutive relationship that relates temperature and the composition of water contacting the glass to the corrosion rate. Currently, H^+ is the only aqueous species that has been found to directly influence the rate via the activity product term [4]. Consequently, Eq. (1) can be simplified to

$$J_i^a = \upsilon_i \vec{k} e^{-\frac{E_a}{RT}} a_{H^+}^{-\eta} \left[1 - \left(\frac{Q}{K}\right)^{\sigma}\right], \quad i = 1, 2, \ldots, N \tag{2}$$

where a_{H^+} is the hydrogen ion activity. Application of Eq. (2) for modeling glass corrosion in a disposal system requires the computation of the chemical affinity term, Q/K, pH, and temperature as a function of time and space, which in our case is being done with the AREST-CT code. Assignment of an appropriate rate-controlling phase and its equilibrium constant (K) is a critical part of the model. Inclusion of all the glass elements in a hypothetical phase has not proven successful in modeling laboratory test data [5,6]. Assigning K to a simple SiO_2 polymorph, such as chalcedony, or mixtures of simple hydroxides and silicate phases [7], has yielded better agreement for most glasses. The stoichiometric coefficients, υ_i, are determined by glass composition, so the remaining four parameters, $\vec{k}$, E_a, η, and σ must be determined from laboratory experiments.

One experimental method that is often used for measuring these physical constants is the single-pass flow-through (SPFT) test. This test has been used to measure reaction rates of minerals [8,9] and glasses [10,11]. The SPFT test is designed to measure reaction rates under tightly controlled, dilute solution conditions. Dilute solution conditions are essential because the dissolution of silicate glasses and minerals in an aqueous solution is subject to the common ion effect, which occurs when a solution already contains the same ions that would be released when a solid dissolves (or precipitates). The presence of common ions released from the glass or from other sources reduces the net rate of release relative to the rate in pure water. Hence, the idea of the SPFT test is to remove the elements released into solution from glass dissolution by continuously introducing fresh water into the system. This maintains the chemical affinity term, Q/K, at a value near zero in Eq. (2). By monitoring the change in dissolution rate over a sufficient range of temperature and pH values, $\vec{k}$, E_a, and η can be easily obtained by applying standard non-linear regression techniques to Eq. (2). Methods for determining the parameter σ have been poorly documented and many studies of silicate mineral dissolution simply assume $\sigma = 1$. We will illustrate how the SPFT test can also be used to obtain information on the parameters associated with the chemical affinity term in the rate law, i.e., σ and K.

Measurement of kinetic rate law parameters using the SPFT method does, however, present an experimental dilemma because solution concentrations must be maintained dilute so that the affinity term, Q/K, remains negligible, but not so dilute that the solution concentrations cannot be determined using standard analytical techniques. One objective of the present work is to show how test conditions meeting these contrasting requirements can be quantified.

3. Experimental

Experimental methods and materials that were used are described in the following sections.

3.1. Materials

The glass used in these studies is identified as LD6-5412 and the composition is given in Table 1. Its most notable feature is the high Na_2O and Al_2O_3 content, about double the Na and two to four times the Al of typical high-level waste glasses. Glass samples were prepared according to standard PCT methods [12]. Most tests were done using a 150 μm to 75 μm

Table 1
Composition of LD6-5412 glass

Oxide	wt%
Al_2O_3	12.00
B_2O_3	5.00
CaO	4.00
K_2O	1.46
Na_2O	20.00
P_2O_5	0.19
SiO_2	55.91
Others	1.44

(−100 + 200 mesh) size fraction but a test series at 40°C was also performed using a 425 μm to 250 μm (−40 + 60 mesh) size fraction and with glass monoliths. Glass density was measured at 2.57 g/cm^3. The glass density was used to compute the change in surface area that occurs over the course of a test. The procedure used for this calculation is given in Appendix A.

Seven different buffer solutions were used to control the pH during the SPFT tests. The composition of each buffer and the computed pH at each of the test temperatures are given in Table 2. It is extremely important to take into account the change in pH that occurs at different temperatures when computing kinetic rate parameters from SPFT data as the at-temperature pH can vary by as much as 2 pH units over the temperature range of 20 to 90°C.

3.2. Test method

A schematic of the single-pass flow-through apparatus used for all the tests discussed in this paper is given in Fig. 1. Although the schematic illustrates only a single cell, our apparatus has a capacity of 24 individual cells and 13 different pH buffers that can be run simultaneously. The apparatus features an indirect flow path, i.e., the aqueous solution is not pumped directly through the sample. This design has two key advantages: (1) bubbles that form in the fluid transfer lines cannot become entrained in the porous glass bed and thus potentially affect the exposed sample surface area, and (2) a gas or gas mixture can continuously flow through the cell. This allows the experimentalist to examine the effects of changing the partial pressure of a gas on the reaction kinetics. Fluid is pumped from the buffer solution reservoir into a tri-port staging vessel where it is transferred periodically by gas pressure. The periodic fluid transfer occurs because fluid will rise in the tri-port vessels until the solution and the fluid line come into contact, closing the gas flow path. Pressure then builds up in the tri-port vessel, which initiates the fluid transfer into the reaction cell in the oven. Fluid will continue to transfer, and thus reduce the height of the solution in the tri-port vessel, until surface tension between the outlet tube and the fluid is overcome. At that point, contact between the outlet tube and the fluid in the tri-port vessel is broken, fluid transfer halts, and gas flow resumes through both the tri-port vessel and the reaction cell.

Although periodic solution replenishment is a common batch experimental technique (such as in the ANS 16.1 test), the practice severely complicates the interpretation of the test results because of the periodic and abrupt change in the solution chemistry that occurs after a replenishment is done. In the SPFT, however, the solution transfer occurs automatically many

Table 2
Composition of buffer solutions used for single-pass flow-through tests. Solution pH and ionic strength values were calculated with the EQ3NR Code V7.2b and the Gembochs V2-EQ8-DataO.com.R2 database. Dissociation constants for TRIS were obtained from Refs. [17,18] and added to the database

Buffer	Composition	I	pH 20°C	pH 40°C	pH 70°C	pH 90°C
1	0.005 m KHphth + 0.0041 m LiOH	0.0132	5.92	5.91	5.90	5.89
2	0.005 m H_3BO_3 + 0.0003 m LiOH	0.0003	8.06	7.91	7.71	7.62
3	0.005 m H_3BO_3 + 0.0020 m LiOH	0.0019	9.07	8.91	8.70	8.59
4	0.005 m H_3BO_3 + 0.0044 m LiOH	0.0044	10.05	9.80	9.46	9.25
5	0.004 m LiCl + 0.001 m LiOH	0.0050	11.11	10.50	9.77	9.39
6	0.005 m LiCl + 0.0107 m LiOH	0.0153	12.12	11.50	10.78	10.39
7	0.01 m TRIS + 0.002 m HCl	0.0020	8.83	8.29	7.63	7.27

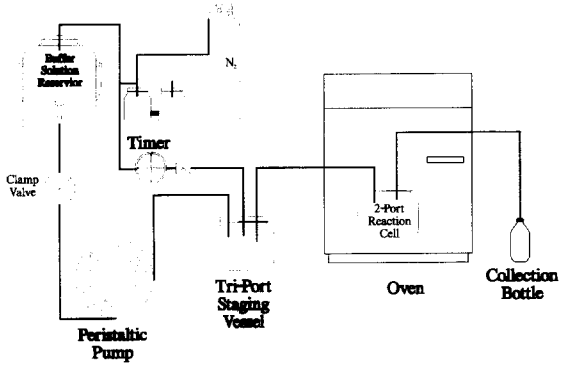

Fig. 1. Schematic of single-pass flow through apparatus.

times each day (depending on the flow rate), and because the solution always remains dilute, the small variation in the solution concentrations that occurs between pulses should not affect the test results.

Effluent from each cell was collected in a bottle that was sampled at selected intervals. At each sample interval, the solution pH was measured, and a sample from each collection bottle was taken and acidified with 1 vol.% of Ultrex nitric acid. Samples from several tests were also filtered using 1.8 nm pore size Centriflo filters (prior to acidification). The acidified samples were then analyzed by ICP-AES. Variations in pH were less than 10% from the nominal pH values of the starting buffer solutions. A minimum of two blank samples was collected on each cell prior to placing the glass samples in the containers. The blank samples were treated in exactly the same manner as the cells with glass samples. Flow rate was determined from gravimetric analysis of the fluid collected in each collection bottle between samplings. Flow rate variations were typically less than 5%. Finally, to independently verify the assumptions made in interpretation of the SPFT data, a series of static dissolution tests were conducted at Argonne National Laboratory at 40°C and a surface area-to-volume ratio (S/V) of about 10 m^{-1} with demineralized water and with buffer #3.

3.3. Test matrices

Two sets of test matrices were run. The first matrix consisted of the nominal data set that covered the four test temperatures and pH range using buffers #1 through #6 given in Table 2. The second matrix was performed only at 40°C and varied the flow rate, particle size, and glass surface area. Most of these tests were done using buffer #3 but a few were replicated in the TRIS buffer #7. As will be discussed later, the data from this second matrix were also used to evaluate parameters associated with the chemical affinity term in Eq. (2).

4. Results

4.1. Analysis method

The normalized release rate was calculated for each component i and at each sampling interval j using the following formula

$$R_{i,j} = \left(C_{i,j} - \overline{C}_{i,b}\right)\frac{q_j}{f_i s_j} \tag{3}$$

where $R_{i,j}$ = normalized rate of ith element at the jth sampling, q_j = flow rate at time period j, m^3/s, $C_{i,j}$ = concentration of component i, at time period j, $\overline{C}_{i,b}$ = mean background concentration of component i, f_i = mass fraction of component i, s_j = average total glass surface area over time period $j-1$ to j, m^2.

A description of the method used to calculate the time-dependent surface area of the glass is given in Appendix A. For the 40°C and 20°C experiments, the mass loss never exceeded more than 2%, so the surface area correction was negligible. However, for the 90°C tests, over 8% mass loss was calculated in one test and the surface area correction for these data did affect the results.

Due to the large volume of SPFT data that has been collected at our laboratory, an automated method was needed to assist in the storage and retrieval of selected data sets and to standardize methods for data reduction. All of the corrosion rate calculations presented in this report were done with the aid of a computer code that acts as a data retrieval and data reduction engine. The single-pass flow-through analyzer (SIPFT) code (pronounced as 'sift') operates by querying a database file that

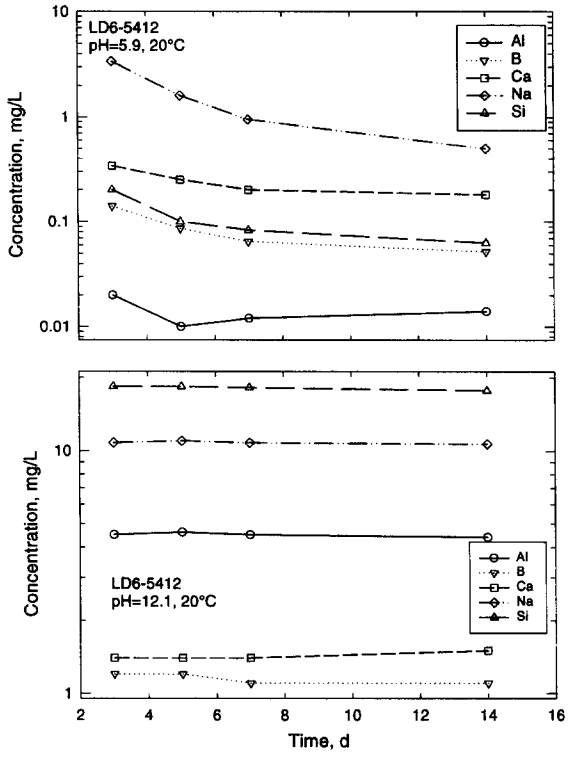

Fig. 2. Solution concentration of selected elements as a function of time.

contains all of the SPFT test results, glass composition, and glass physical property data. This database currently contains approximately 1000 records, representing well over 20,000 individual data entries. The query then returns a record set that matches the criteria specified by the user. There are also options for displaying the data in raw concentration units, as normalized rates, and to correct for background subtraction, surface area changes, and chemical affinity in computing the rate. The correction for chemical affinity is currently limited to simple SiO_2 polymorphs (such as chalcedony) where the values for K are interpolated from values provided in the EQ3/6 database, or optionally defined by the user.

4.2. Solution concentration results

Many of the trends in the time-dependence of the solution concentration results were essentially identical among the tests. Consequently, only selected examples will be presented here to illustrate the major features. Fig. 2 shows the time-dependent change in the solution concentration of each major glass component as a function of time in the pH 6 and pH 12 buffers at 20°C. Note that at the low pH, steady state has not quite been achieved through 14 days test duration. However, at pH 12,

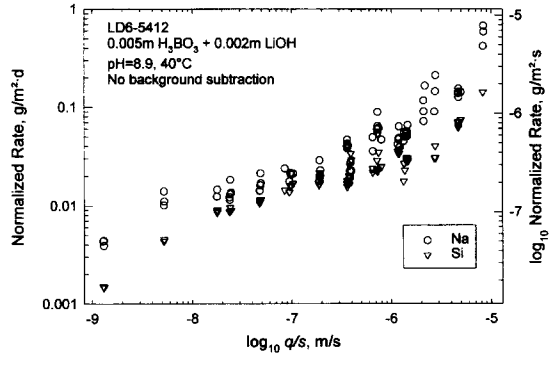

Fig. 3. Normalized release rate as a function of q/s neglecting background subtraction.

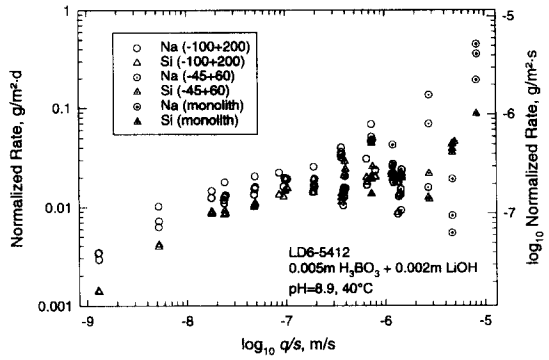

Fig. 4. Normalized release rate as a function of q/s including background subtraction.

steady-state solution concentrations are observed even at the first sampling taken after 3 days. Similar trends were observed in the tests run at 40, 70, and 90°C.

4.3. Corrosion rate results

4.3.1. Effect of q/s

Fig. 3 shows the calculated normalized release rate of both Na and Si as a function of the parameter q/s when the raw solution concentration data have not been background subtracted in accordance with Eq. (3). As is clearly evident, the computed release rates for both Na and Si appear to continuously increase with increasing flow rate (or decreasing glass surface area). However, as documented by McGrail and Peeler [13], this phenomenon is due to the omission of background subtraction in computing the normalized rate and so has no physical significance. As Fig. 4 illustrates, once proper background subtraction is applied to the raw data, the apparent flow rate dependence of the normalized rate disappears, at least at $q/s \geq 5 \times 10^{-8}$ m/s.

The data in Fig. 4 are also separated in terms of the mesh size fraction used in the test. As is apparent from the data, there is no measurable difference or bias in the results for the different mesh sizes versus the tests with monolith samples.

The increasing scatter in the calculated release rates for both Na and Si as q/s increases beyond 10^{-6} m/s is due to the combination of increasing analytical uncertainty as the solutions become more dilute and the multiplication of these increasingly uncertain values by larger and larger values of q/s in computing a dissolution rate with Eq. (3). Analytical uncertainty was quantitatively investigated by computing a two sample t-statistic assuming unequal variances between the blank sample population and four samples obtained from each test. These data are plotted in Fig. 5. A t-statistic < -3 indicates that the mean of the test samples is larger than the mean of the blank sample population at the 95% confidence level. As is apparent from Fig. 5, at $q/s > \sim 5 \times 10^{-7}$ m/s for Na and 10^{-6} m/s for Si, there is no statistically significant difference between the sample populations. Consequently, the calculated normalized rates are not reliable at q/s values that exceed these limits.

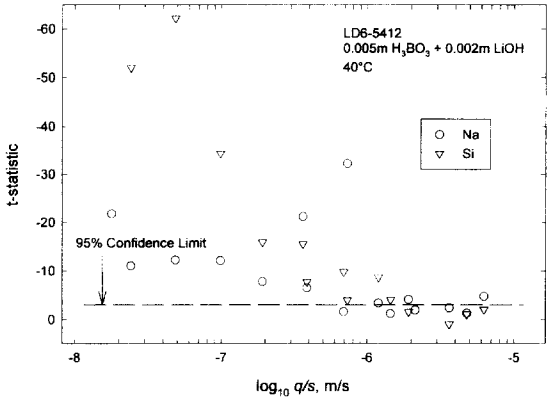

Fig. 5. Computed t-statistic for Na and Si as a function of q/s.

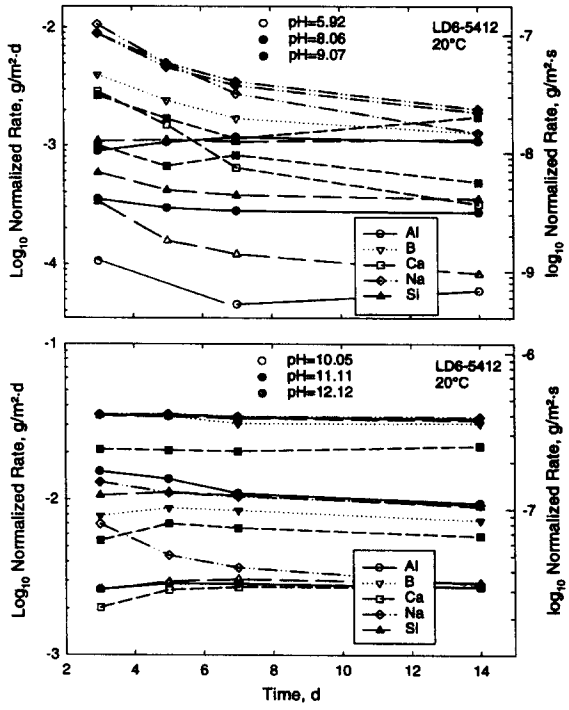

Fig. 6. Normalized release rate as a function of time for selected elements at 20°C.

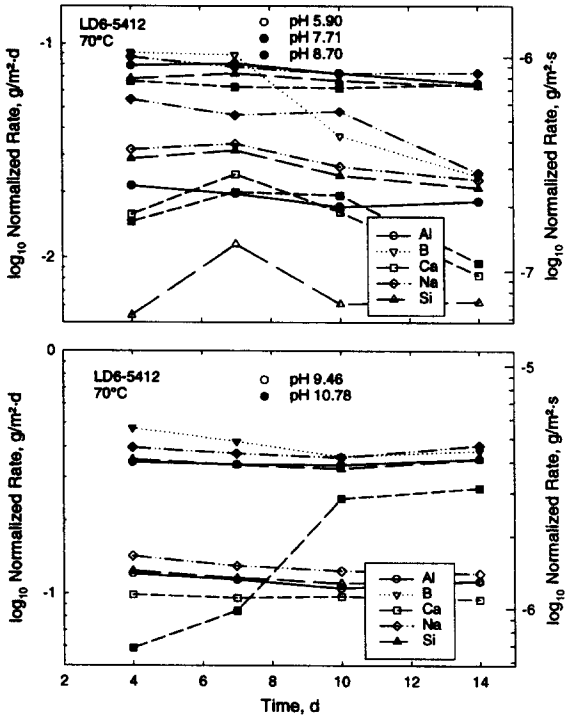

Fig. 7. Normalized release rate as a function of time for selected elements at 70°C.

4.3.2. Effect of pH and temperature

Fig. 6 shows the calculated normalized release rate data at 20°C for buffers 1 through 6, where background and surface area corrections have been applied but not for chemical affinity. At pH 5.9, the glass dissolution is non-stoichiometric with enhanced release rates of both Na and B throughout the 14 day test duration. The release rates also decrease continuously with time. The glass dissolution is essentially stoichiometric, with the exception of Na, at all the other pH values tested, particularly at the longer test durations. The Na release rate is independent of pH, until the pH reaches 10. These data clearly indicate that Na is being released from LD6-5412 glass by at least two independent processes. One process is, of course, matrix dissolution. The second is most likely an ion-exchange reaction. At low temperature (20°C) and near neutral pH, ion exchange is the dominant release mechanism for Na. Matrix dissolution does not become the dominant release mechanism until the pH $\geq$ 10.

Fig. 7 shows the calculated normalized release rate at 70°C. Again, at pH 5.9, incongruent dissolution is observed. At the other pH values tested, the glass dissolution is essentially stoichiometric. Unlike the experiments at 20°C, however, the Na release rate is not discernibly higher than the release rates of the other glass components for pH values greater than 7. Matrix dissolution is a more thermally activated process than ion exchange and so the matrix dissolution rate increases faster with increasing temperature as compared with ion exchange. Consequently, enhanced Na release from ion exchange is masked at lower pH values in tests at 70°C than in tests at 20°C.

5. Discussion

Before utilizing the normalized release rate results presented in Section 4.3 to compute the kinetic rate law parameters ($\vec{k}$, E_a, η), it must be demonstrated that the formation of secondary phases did not significantly alter the measured solution concentrations of the glass components, particularly Si. Scanning electron microscopic analysis of selected glass samples after test termination showed no evidence of secondary phase formation. However, geochemical modeling was also used to evaluate the saturation state of the aqueous phase with respect to key minerals in the database.

5.1. Geochemical code simulations

The parameter $\log_{10} Q/K$, or saturation index, was computed for the conditions of the SPFT tests with the aid of the geochemical code EQ3/6 V7.2b (Wolery, 1992) and using the database GEMBOCHS.V2-EQ8-DATA0.COM.R2. Fig. 8 shows the results for the pH 8 buffer at 20°C. The vertical line is the maximum value of reaction progress (mol of glass per kg of H_2O) achieved in the SPFT test that was calculated from the maximum concentration of Si measured in the effluent. The horizontal line is drawn at a $\log Q/K = 0$ indicating saturation with respect to a solid phase. The curves are the computed saturation indices for each mineral phase assuming the glass dissolves congruently. Sodium was found to be preferentially released at early times in our experiments, so this computational procedure will underestimate the saturation indices for solid phases that contain Na. However, almost all of these phases were many orders of magnitude undersaturated, so correcting for the early-time, incongruent release of Na was not considered important. Curves falling inside the shaded box indicate supersaturation with respect to the phase and thus the *potential* for precipitation of the phase in the experiment. Careful interpretation of these calculations is required because many factors contribute to the nucleation and growth of a

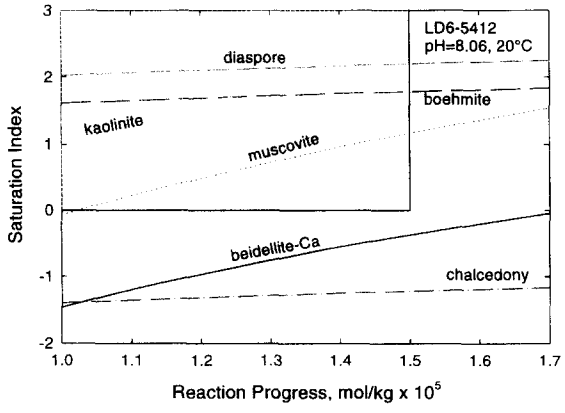

Fig. 8. Calculated saturation indices for selected mineral phases in a SPFT test with LD6-5412 glass in 0.005 m H_3BO_3 + 0.0003 m LiOH solution at 20°C.

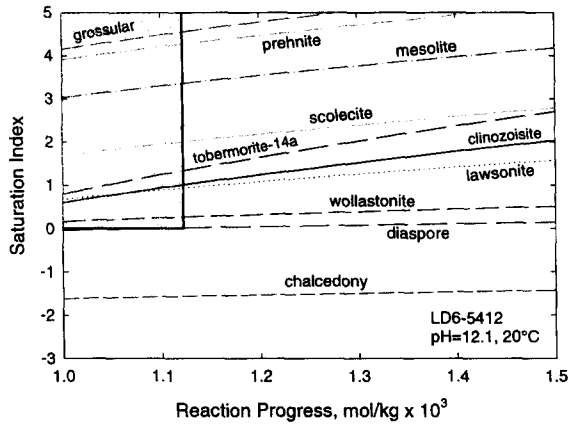

Fig. 9. Calculated saturation indices for selected mineral phases in a SPFT test with LD6-5412 glass in 0.005 m LiCl + 0.0003 m LiOH solution at 20°C.

secondary phase, including kinetic constraints on precipitation. Also, at temperatures ≥ 40°C, direct measurement of the solubility products for minerals in the database is sparse. Extrapolation techniques are then used to compute equilibrium constants, which increases the uncertainty in the computed saturation indices. Still, the calculations provide an extremely useful, if not fully quantitative, analysis of whether the desired conditions of the SPFT test were actually achieved.

For the test shown in Fig. 8, four mineral phases compute as being supersaturated. However, simulations of the SPFT tests where these phases are allowed to precipitate produce solution concentrations of Ca, Al, and Si that are much lower than the values measured in the tests. Colloid formation could account for the computed supersaturation with respect to the phases containing Al. However, none of the samples that were filtered showed evidence of colloids, including samples taken at the smallest values of q/s (highest solution concentrations). It is also important to note that none of these phases have been found to be consistent with modeling long-term static experiments with this glass. Consequently, it is unlikely that any of these supersaturated phases formed in the test. The saturation index of chalcedony is $\sim 10^{-1.3}$ at the maximum value of reaction progress. Although the solution is undersaturated with respect to this phase, a chemical affinity correction may be justified depending on the value for the reaction order parameter, σ, and whether the log K for chalcedony is appropriate for LD6-5412 glass. This will be examined in Section 5.2.

Fig. 9 shows the computed saturation indices for the pH 12 buffer at 20°C. Ten secondary solids were computed as being supersaturated in this case. However, the formation of only one of the phases, hydroxylapatite [$Ca_5OH(PO_4)_3$] (not shown on Fig. 9) was found to be consistent with the measured solution concentration data when allowed to precipitate in the simulations. Consequently, it is unlikely that any of the other supersaturated secondary solids formed in this test. The saturation index for chalcedony in this case is $\sim 10^{-1.6}$ indicating that an affinity correction may be justified, again depending on values for σ and K. Calculations were also done at other temperatures and for each buffer solution. The results from these calculations were all very similar to the results presented in Figs. 8 and 9.

5.2. Determination of chemical affinity parameters σ and K

We begin the discussion of how SPFT tests may be used to determine the chemical affinity parameters (σ and K) by first writing a general mass balance for the time-dependent concentration of an element i in the effluent from a SPFT cell

$$V\frac{dC_i}{dt} = v_i s\vec{k}a_{H^+}^{-\eta(T)}e^{-\frac{E_a}{RT}}\left[1-\left(\frac{Q(t)}{K}\right)^{\sigma}\right] - q\left(C_i - \overline{C}_{i,b}\right), \tag{4}$$

where C_i is the concentration of component i, and V is the static volume of water in contact with glass (m^3).

Eq. (4) is valid assuming congruent dissolution of the glass and that no secondary solids form containing the element of interest. For a series of SPFT tests conducted at one temperature and in one buffer solution, Eq. (4) reduces to

$$V\frac{dC_i}{dt} = v_i s k_0\left[1-\left(\frac{Q(t)}{K}\right)^{\sigma}\right] - q\left(C_i - \overline{C}_{i,b}\right), \tag{5}$$

where k_0 is a rate constant.

If we make an assumption that the rate-controlling phase is a simple SiO_2 polymorph and invoke the dilute solution approximation so that thermodynamic activities can be replaced with concentrations, Eq. (5) simplifies further to

$$V\frac{dC_i}{dt} = v_i s k_0\left[1 - \left(\frac{C_{Si}}{C^*_{Si}}\right)^{\sigma}\right] - q\left(C_i - \overline{C}_{i,b}\right), \tag{6}$$

where C^*_{Si} is the concentration of Si in the buffer solution at equilibrium with respect to the SiO_2 polymorph. For the case where i = Si, Eq. (6) becomes

$$V\frac{dC_{Si}}{dt} = v_{Si} s k_0\left[1 - \left(\frac{C_{Si}}{C^*_{Si}}\right)^{\sigma}\right] - q\left(C_{Si} - \overline{C}_{Si,b}\right). \tag{7}$$

Using the initial condition $C_{Si}(0) = 0$, Eq. (7) can be solved numerically for the case where $0 < \sigma < 1$. However, the analytical solution to Eq. (7) for case where $\sigma = 1$ is of interest because it provides the maximum time to achieve steady-state concentrations in the SPFT test. The analytical solution is

$$C_{Si}(t) = \frac{C^*_{Si}\left(q\overline{C}_{Si,b} + v_{Si} s k_0\right)}{qC^*_{Si} + v_{Si} s k_0}\left(1 - e^{-(1/V)(q + v_{Si} s k_0 / C^*_{Si})t}\right). \tag{8}$$

If steady state is defined as the point where the exponential term equals 0.95, the time to steady-state (t_{ss}) is simply

$$t_{ss} = \frac{3V}{q + v_{Si} s k_0 / C^*_{Si}}. \tag{9}$$

The maximum time to steady state will be in the monolith tests (smallest surface area) run at the lowest flow rate. Substituting appropriate physical constants into Eq. (9) for these tests at 40°C (V = 30 ml, $q = 2.9 \times 10^{-4}$ ml/s, $v_{Si} = 0.26$, $s = 2.5 \times 10^{-4}$ m^2) and, as will be shown in a moment, regressed values for $k_0 = 1.6 \times 10^{-7}$ g/m^2 · s, and $C^*_{Si} = 3.8$ mg/l, the computed t_{ss} is 3.1 days. Since all of the tests were run to times of 14 days, steady-state solution concentrations should have been attained.

In the steady state, Eq. (7) reduces to

$$\frac{1 - \left(C_{Si}/C^*_{Si}\right)^{\sigma}}{C_{Si} - \overline{C}_{Si,b}} - \frac{1}{v_{Si} k_0}\frac{q}{s} = 0. \tag{10}$$

This transcendental equation is not amenable to a closed-form solution for the case where $0 < \sigma < 1$. So, a Marquardt–Levenberg non-linear regression was performed to compute values for k_0, C^*_{Si} and σ. The results gave $k_0 = 1.55 \times 10^{-7} \pm 2.31 \times 10^{-9}$ g/m^2 · s, $C^*_{Si} = 3.82 \pm 0.04$ g/m^3, and $\sigma = 1$. No error bounds are provided for σ because the regression was constrained to fit values of $\sigma \leq 1$, and the best fit was obtained with $\sigma = 1$. The regressed coefficients were substituted into Eq. (10) and the resulting values of C_{Si} as a function q/s are plotted in Fig. 10. Although the fit to the data is excellent (R^2 of 0.996), the physical meaning of C^*_{Si} is not clear because the regressed value is about 1.5 times less than the calculated Si

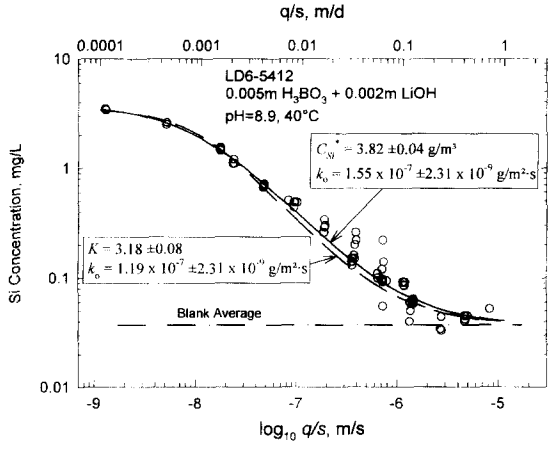

Fig. 10. Comparison of calculated and measured Si concentrations as a function of q/s. The solid line (————) was computed from Eq. (10) and the dashed line (- - -) from Eq. (12a) using the indicated regression parameters.

concentration in this buffer solution in equilibrium with quartz. These results also contrast with a previous study by Bourcier et al. [14] who reported $\sigma = 0.1$ by fitting the rate Eq. (2) to static test data on a glass very similar to LD6-5412.

The low apparent value of C_{Si}^{*} developed from the SPFT data may mean that the assignment of a simple SiO_2 polymorph to the chemical affinity term in the rate law is not appropriate for this glass. Gin [15] has also reported inconsistencies with the use of just SiO_2(aq) in the rate law when modeling SPFT test data on high-level waste glass R7T7 and proposed including Al in the rate law to correct these deficiencies. However, Gin [15] did not present the formal mathematics required to analyze SPFT data using a mixed Si–Al model, so we will do so here. Returning to Eq. (5), but assuming steady-state conditions apply, we can write

$$v_{Si}k_0\left[1-\left(\frac{C_{Si}^{\alpha}C_{Al}^{\beta}}{K}\right)^{\sigma}\right]-\frac{q}{s}\left(C_{Si}-\overline{C}_{Si,b}\right)=0, \tag{11a}$$

$$v_{Al}k_0\left[1-\left(\frac{C_{Si}^{\alpha}C_{Al}^{\beta}}{K}\right)^{\sigma}\right]-\frac{q}{s}\left(C_{Al}-\overline{C}_{Al,b}\right)=0. \tag{11b}$$

The five regression coefficients, k_0, K, α, β and σ, can be obtained by solving a coupled non-linear regression problem in which the coupled non-linear Eqs. (11a) and (11b) must be repeatedly solved simultaneously for values of C_{Si}, C_{Al}, and their partial derivatives with respect to each fitting coefficient. We have not attempted to conduct such an analysis because with five adjustable coefficients, it is virtually guaranteed that suitable parameters can be found that model the data well. An alternative approach is to make an assumption about the values of α, β and σ. For example, Gin [15] assigned α and β to the stoichiometric coefficients for Si and Al, respectively, in the bulk glass. However, this assignment is purely arbitrary. An approach that is more consistent with the mechanism of the glass dissolution process is to assume that the activated complex may involve the formation of key structural group, such as an $AlSiO_4^-$ group ($\alpha = \beta = 1$), for example. If we further assume that $\sigma = 1$, which provided the best fit when using a simple SiO_2 polymorph in the rate law, then an analytical solution to Eqs. (11a) and (11b) can be derived

$$C_{Si}=\frac{v_{Al}k_0\overline{C}_{Si,b}-v_{Si}k_0\overline{C}_{Al,b}-(qK/s)+B}{2v_{Al}k_0}, \tag{12a}$$

$$C_{Al}=\frac{v_{Si}k_0\overline{C}_{Al,b}-v_{Al}k_0\overline{C}_{Si,b}-(qK/s)+B}{2v_{Si}k_0}, \tag{12b}$$

where B is

$$B=\sqrt{4v_{Si}k_0K\left(v_{Al}k_0+\frac{q\overline{C}_{Al,b}}{s}\right)+\left(v_{Al}k_0\overline{C}_{Si,b}-v_{Si}k_0\overline{C}_{Al,b}+\frac{qK}{s}\right)^2}. \tag{13}$$

Eq. (12a) was fit to the data shown in Fig. 10 and the results are plotted (dashed line) along with the regressed values for k_0 and K. Using these same coefficients, C_{Al} as a function of q/s was computed using Eq. (12b) and the results are plotted in Fig. 11, along with the Al concentration data from the SPFT tests. The computed curve with the mixed Si–Al model is

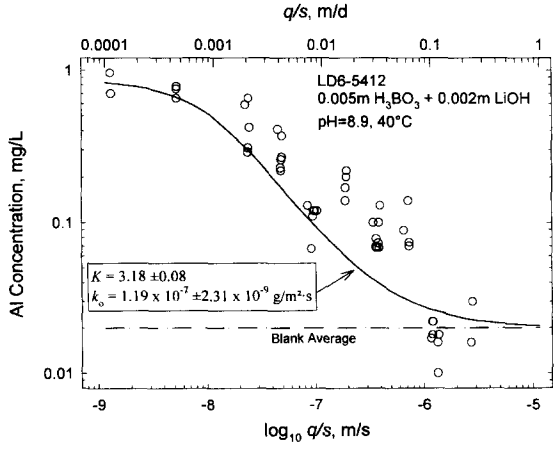

Fig. 11. Comparison of calculated and measured Al concentrations as a function of q/s. The solid line (————) was computed from Eq. (12b) using the indicated regression parameters.

essentially identical to the simpler model using just Si in the rate law. We also derived analytical solutions to Eqs. (11a) and (11b) for cases where $\alpha = 2$, $\beta = 1$ and $\alpha = 1$, $\beta = 2$. In both cases, the calculated C_{Si} and C_{Al} as a function of q/s were almost identical to the curves shown in Figs. 10 and 11 for $\alpha = \beta = 1$. The simple flow rate variations used in our study do not provide the necessary or sufficient data to distinguish between different forms of the mixed Si–Al rate law. Additional experiments are needed where one of the dependent variables (C_{Si} or C_{Al}) is held constant while the other is varied over an appropriate concentration range. The analytical solution (Eqs. (12a) and (12b)) should be very useful in developing an appropriate experimental design for these tests.

5.3. Determination of $\vec{k}$, E_a and η

Fig. 12 shows the computed normalized Si release rate as a function of the computed pH at temperature for each of the buffer solutions used. We selected Si as the primary element for the determination of the rate law constants as it is the major glass matrix component and did not have interferences with any of the buffer components. The chemical affinity correction option in the SIPFT code was used in the rate computations using the regressed parameters k_0 and C_{Si} as determined in Section 5.2, and assuming the temperature dependence of C_{Si}^* follows that of quartz. The data for the TRIS buffer tests at 40°C (pH 8.29) are consistent with the data for the 0.005 m H_3BO_3 + 0.0003 m LiOH buffer (pH 7.91), indicating that the buffer components are not affecting the measured release rates.

A linear regression to the data at each temperature gave $\eta = 0.40 \pm 0.03$ indicating that η does not depend on temperature within experimental error. By assuming $Q/K = 0$ in Eq. (2), a non-linear regression was performed using the entire SPFT data set, with the exception of the pH 5.9 data at 40°C. The resulting regression coefficients are $\log_{10}\vec{k} = 2.05 \pm 0.16$ g/m^2 s and $E_a = 74.8 \pm 1.0$ kJ/mol with a correlation coefficient (R^2) of 0.97, indicating an excellent fit to the data set. This is also apparent by inspection of Fig. 12 where the lines in the figure do not represent a linear regression to the data at each temperature but were computed from the rate Eq. (2) using the regressed coefficients for $\vec{k}$, E_a and η. The regressed activation energy is typical of reported values for a wide range of borosilicate waste glass compositions.

There is not yet a satisfactory explanation for the pH dependence of the corrosion rate measured in SPFT tests. However, the rate most likely depends on the concentration of oxo, hydroxo, and aquo sites at the surface of the glass that varies as a function of pH. Recent advances in computerized molecular mechanics may be used to predict stability constants for proton binding at oxide surfaces [16]. With these stability constants, it is hoped that pH dependence of the rates observed in the SPFT test can be predicted from first principles.

5.4. Comparison with static dissolution tests

Fig. 13 shows the values of normalized mass loss (NL) of Na and Si measured with static tests conducted at 40°C in buffer #3. The normalized release rate is given by the slope of the lines, which was determined from a linear regression to the 3, 5, 7, and 10 day results for Si. A line through the Na data was fit by constraining the slope to same value computed for the Si data, but allowing the y-intercept to increase to account for the initially high transient release of Na. The regressed normalized release rate of $2.9 \times 10^{-7} \pm 1.9 \times 10^{-7}$ g/m^2 s is within experimental error of the k_0 value of $1.6 \times 10^{-7} \pm 2.3 \times 10^{-9}$ g/m^2 s computed from the SPFT data (Fig. 10). Both NL(Na) and NL(Si) fall below the regression line at reaction times longer than about 10 days, which corresponds to a Si concentration of about 0.6 mg/l. This value is also in excellent agreement with the SPFT test results (Fig. 4) that show a decrease in the rate in tests run at a q/s less than 6×10^{-8} m/s that had Si concentrations of approximately 0.7 mg/l or larger (see Fig. 10).

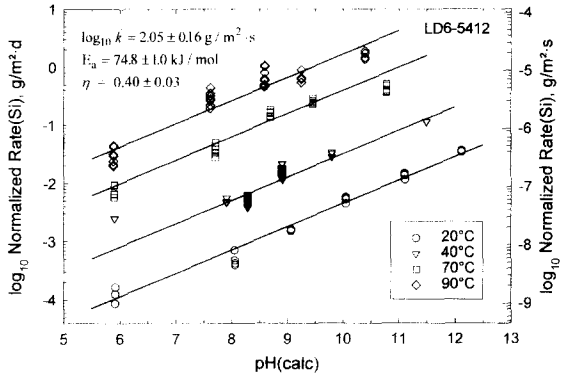

Fig. 12. Normalized Si release rate as a function of pH and temperature.

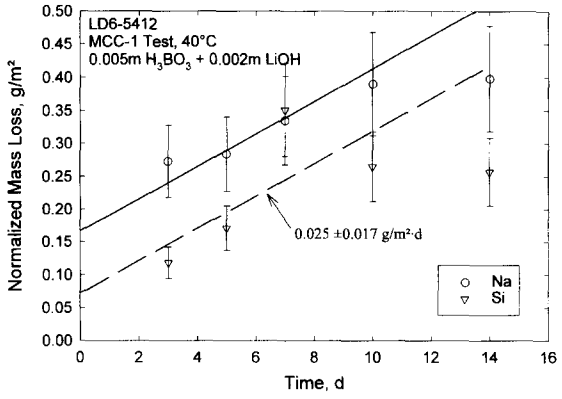

Fig. 13. NL(Na) and NL(Si) versus reaction time for static dissolution tests at 40°C and 10 m^{-1} with LD6-5412 glass in buffer #3.

For this set of batch experiments, the linear regression to the Si release data produced a large uncertainty in the rate ($\pm 68\%$). The SPFT technique is preferred for kinetic rate law parameter measurements because it (1) typically generates a larger data density, (2) inherently minimizes transient effects (such as the initial burst release of Na) by fluid replenishment and by being able to run the test for longer times, and (3) maintains fixed solution chemistry. All of these factors 19 tend to minimize uncertainty associated with rate constant determinations as compared with using batch experimental methods.

6. Conclusion

A suite of single-pass flow-through measurements was completed with a Na–Ca–Al borosilicate glass being studied as part of a program to immobilize low-activity waste. Forward reaction rates were determined over a temperature range of 20 to 90°C and pH range of 6 to 12. Non-linear regression techniques were applied to a kinetic rate law to obtain three fundamental physical constants that are required for modeling the corrosion kinetics of this glass. These three physical constants are the intrinsic rate constant ($\vec{k}$), activation energy (E_a), pH power law coefficient (η). The values of these three constants for LD6-5412 glass were found to be $\log_{10}\vec{k} = 2.05 \pm 0.16$ g/m^2 s, $E_a = 74.8 \pm 1.0$ kJ/mol, $\eta = 0.40 \pm 0.02$. By varying the ratio of flow rate to surface area (q/s) in SPFT tests, a quantitative method was also described to evaluate the reaction order parameter (σ) and pseudoequilibrium constant (K) associated with the chemical affinity term in the rate law. An analytical solution to the mass balance equation(s) that describe the variation in effluent concentrations as a function q/s was derived for a simple model where the chemical affinity term is assumed to follow a first order dependence on the concentration of Si only and for a more complex model including both Si and Al. Finally, static dissolution tests were used to independently verify the results from the SPFT data analysis procedures and to help identify the optimal conditions for conducting the tests.

Appendix A. Computation of surface area change from flow-through data

Nomenclature

Variables

C concentration, g/m^3
m mass, g
N number of glass particles
q flow rate, m^3 s
r radius of glass particle, m
s surface area, m^2
t time, s

Greek symbols

Δ difference operator
π pi
ρ glass density, g/m^3

Subscripts

i,j time period
k glass component, B, Si, etc.
0 reference value at time zero

The purpose of this note is to illustrate a computational procedure for computing the change in glass surface area that occurs during glass corrosion tests, such as the SPFT test. The analysis presented here is intended for use in tests where the glass has been ground and sieved to a specific mesh size. We assume here that the ground glass is adequately represented by spherically-shaped particles.

With the above assumptions, the total surface area of the glass at a time interval i, is given by

$$s_i = 4\pi N r_i^2. \tag{A.1}$$

Eq. (A.1) can be written in terms of variables that are known, namely the glass density and total mass by a simple change of variables. We first need an expression for N. This can be found by realizing that

$$m_0 = \frac{4}{3} N \pi \rho r_0^3. \tag{A.2}$$

Solving Eq. (A.2) for N gives

$$N = \frac{3m_0}{4\pi\rho r_0^3}. \tag{A.3}$$

Substituting Eq. (A.3) into Eq. (A.1) gives

$$s_i = \frac{3m_0}{\rho r_0^3} r_i^2. \tag{A.4}$$

The remaining unknown, r_i, can be eliminated from Eq. (A.4) by first writing an expression for the total mass of glass at any time i that is analogous to Eq. (A.2)

$$m_i = \frac{4}{3} N \pi \rho r_i^3. \tag{A.5}$$

Substituting Eq. (A.3) into Eq. (A.5) gives

$$m_i = m_0 \frac{r_i^3}{r_0^3}. \tag{A.6}$$

Solving Eq. (A.6) for r_i,

$$r_i = \left(\frac{m_i}{m_0} \right)^{1/3} r_0. \tag{A.7}$$

Substituting Eq. (A.7) into Eq. (A.4) we arrive at the following expression

$$s_i = \frac{3}{\rho r_0} m_0^{1/3} m_i^{2/3}. \tag{A.8}$$

Eq. (A.8) provides an expression for the surface area at time i once m_i has been computed.

For a single-pass flow-through test, this is done with the following expression:

$$m_i = m_0 - \frac{1}{f_k} \left[\sum_{j=1}^{i-1} q_j C_{j,k} \Delta t_j + q_i C_{i,k} \frac{\Delta t_i}{2} \right], \quad i \geq 1. \tag{A.9}$$

Eq. (A.9) represents a time-centered approximation to the total mass at the current time step. The summation term represents the accumulated mass loss up to time step $i-1$ and the second term in the brackets represents $1/2$ of the total mass loss from time $i-1$ to i. This expression is readily implemented in a spreadsheet program or other computational software. The element concentration used in Eq. (A.9) for the mass loss calculation should be an element such as B, Na, or Si that is expected to be most representative of the true amount of glass dissolved in the test.

References

[1] B.P. McGrail, L.A. Mahoney, Selection of a Computer Code for Hanford Low-Level Waste Engineered-System Performance Assessment, PNL-10830, Pacific Northwest Laboratory, Richland, WA, 1995.
[2] B.P. McGrail, C.I. Steefel, J.A. Fort, D.W. Engel, S.B. Yabusaki, Mater. Res. Soc. Symp. Proc. 353 (1995) 551.
[3] P. Aagaard, H.C. Helgeson, Am. J. Sci. 282 (1982) 237.
[4] W.L. Bourcier, H.C. Weed, S.N. Nguyen, J.K. Nielsen, L. Morgan, L. Newton, K.G. Knauss, in: Proc. 7th Annual Water-Rock Interaction Conf., Balkema, Rotterdam, 1992, pp. 81–84.
[5] W.L. Bourcier, Geochemical Modeling of Radioactive Waste Glass Dissolution Using EQ3/6: Preliminary Results and Data Needs, UCID-21869, Lawrence Livermore National Laboratory, Livermore, CA, 1989.
[6] T. Advocat, J.L. Crovisier, B. Fritz, E. Vernaz, Mater. Res. Soc. Symp. Proc. 176 (1990) 241.
[7] W.L. Bourcier, D.W. Peiffer, K.G. Knauss, K.D. McKeegan, D.K. Smith, Mater. Res. Soc. Symp. Proc. 176 (1990) 209.
[8] K.G. Knauss, T.J. Wolery, Geochim. Cosmochim. Acta 50 (1986) 2481.
[9] P.M. Dove, D.A. Crerar, Geochim. Cosmochim. Acta 54 (1990) 955.
[10] K.G. Knauss, W.L. Bourcier, K.D. McKeegan, C.I. Merzbacher, S.N. Nguyen, F.J. Ryerson, D.K. Smith, H.C. Weed, L. Newton, Mater. Res. Soc. Symp. Proc. 176 (1990) 371.
[11] B.P. McGrail, K.M. Olson, Evaluating Long-term Performance of In-situ Vitrified Waste Forms: Methodology and Results, PNL-8358, Pacific Northwest Laboratory, Richland, WA, 1992.
[12] ASTM, Standard Test Methods for Determining the Chemical Durability of Nuclear Waste Glasses: The Product Consistency Test (PCT), ASTM C1285-94, Annual Book of ASTM Standards, Philadelphia, PA, 1994.
[13] B.P. McGrail, D.K. Peeler, Evaluation of the Single-Pass Flow-Through Method to Support a Low-Activity Waste Specification, PNL-10746, Pacific Northwest Laboratory, Richland, WA, 1995.
[14] W.L. Bourcier, S.A. Carroll, B.L. Phillips, Mater. Res. Soc. Symp. Proc. 333 (1994) 507.
[15] S. Gin, Mater. Res. Soc. Symp. Proc. 412 (1996) 189.
[16] J.R. Rustad, B.P. Hay, Geochim. Cosmochim. Acta 107 (1995) 433.
[17] R.G. Bates, H.B. Hetzer, J. Phys. Chem. 65 (1961) 667.
[18] S.P. Datta, A.K. Grzybowski, B.A. Weston, J. Chem. Soc. (1963) 792.